Engineering Turbulence Modelling and Experiments 3
W. Rodi and G. Bergeles (Editors)

Numerical Study of Effusion Cooling in a Double-Row Discrete-Hole Configuration Using a Low-Re Reynolds Stress Transport Model

L.S. Jansson and L. Davidson
Thermo and Fluid Dynamics
Chalmers University of Technology
S-412 96 Gothenburg
Sweden

Abstract[1]

The paper presents numerical simulations of a discrete-hole cooling flow field with relevance to gas turbine film-cooling. Predictions are made of the three-dimensional turbulent flow generated by two rows of inclined jets in a staggered arrangement issuing from circular outlets in a wall into a free stream along this wall. A Reynolds Stress Transport Model (RSTM) is used. In the near-wall region a slightly modified version of the low-Re RSTM of Shima [1] is used. For comparison, a two-layer $k-\varepsilon$ is also used. The flow field properties that are considered in this study are the mean velocities, the turbulent stresses and the adiabatic film-cooling effectiveness for a blowing rate $M = 0.5$ at an injection angle $\alpha = 30^o$ through a plane wall. The predictions are compared to the measurements of Jubran [2].

1. Introduction

The steady increase in the combustor exit gas temperature of gas turbine engines, in order to increase efficiency, clearly indicates that intensive cooling of the turbine blades is required. Hence, the requirement to develop efficient cooling systems, capable of performing better cooling with the available air. Full-coverage discrete hole film-cooling, often referred to as effusion cooling, is a relatively simple technique for efficient cooling of combustor walls and turbine blades. Secondary coolant air on its passage through multiple rows of inclined discrete holes cools the wall convectively and then emerges as a film in the region of the jet exits and thereby protects the surface from the hot main stream.

It is found in the literature that maximum film-cooling effectiveness in the vicinity of the jet exit is achieved with a blowing rate below $M = 0.5$. A blowing rate above this value results in lower cooling effectiveness since the flow emerging from the holes is totally lifted off the surface, allowing the free stream to flow under the injectant flow, thereby reducing the cooling of the surface. However, further downstream of the hole exits, cooling effectiveness tends to increase with the increasing blowing rate, where the jets reattach to the surface. Furthermore the turbulence in the region above the hole is found to be very

[1]The financial support from NUTEK is great-fully acknowledged

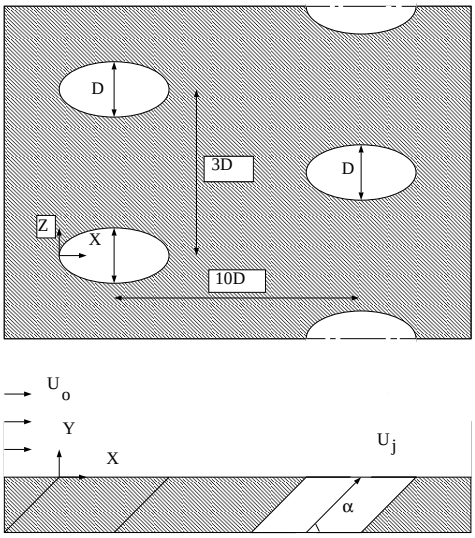

Figure 1. Flow configuration.

anisotropic. Hence, to numerically simulate the flow field, the turbulence model should take the anisotropy of the turbulence into account, and therefore a second-order-closure model should be used. Although the essential characteristics of the thermal and velocity field can be understood from a single-row (or for that matter a single hole) injection, studies of multiple-row injection are important from a design point of view.

There are a few earlier numerical studies of jets in cross flow [3,4] using second-moment closures. In none of these studies were the Reynolds stresses solved all the way to the wall. No work has been found in the literature where second-moment closures have been applied to effusion cooling flows.

2. The Numerical Method

A finite volume code CALC-BFC (Boundary - Fitted - Coordinates) [5] is used. The main features are the use of general curvilinear coordinates, pressure correction scheme (SIMPLEC) [6], Cartesian velocity components as principal unknowns, and colocated grid arrangement together with Rhie and Chow interpolation [7]. In the mean flow equations, the third-order accurate QUICK [8] discretization scheme is adopted and the transport equations for the turbulent quantities are discretized using a second-order accurate bounded scheme by van Leer [9].

3. The Reynolds Stress Transport Model

The time-averaged Reynolds stress transport equation can be written [10]:

$$\frac{\partial}{\partial x_k}\left(\rho U_k \overline{u_i u_j}\right) = P_{ij} + D_{ij}^{L} + D_{ij}^{T} + \Phi_{ij} - \frac{2}{3}\rho\delta_{ij}\varepsilon \qquad (1)$$

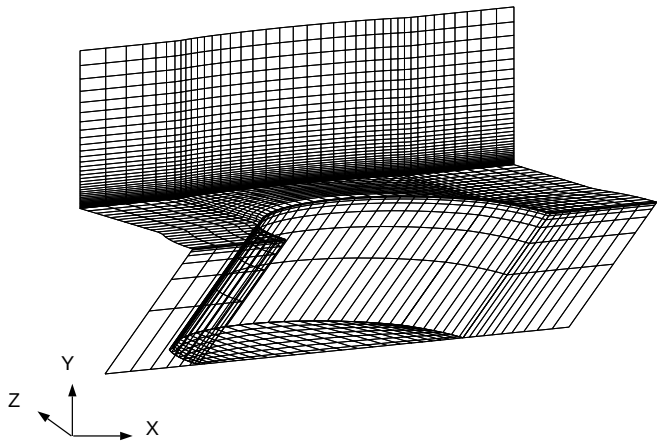

Figure 2. Zoomed view of the grid near the exit of the first jet.

The turbulent kinetic energy is obtained as half the trace of $\overline{u_i u_j}$, i.e. $k = \overline{u_i u_i}/2$. The simplest proposal forms, used for most complex flow computations, are the following relations by Rotta [11] and Naot *et al.* [12]:

$$\Phi_{ij} = \phi_{ij,1} + \phi_{ij,2} + \phi_{ij,w} \; ; \; \phi_{ij,1} = -c_1 \rho \frac{\varepsilon}{k} \left(\overline{u_i u_j} - \frac{2}{3}\delta_{ij} k \right) ; \; \phi_{ij,2} = -c_2 \left(P_{ij} - \frac{2}{3}\delta_{ij} P_k \right) \quad (2)$$

where P_{ij} and P_k are the production of stresses and kinetic energy, respectively. The third term $\phi_{ij,w}$ in Eq. 2a represents the redistribution due to the effects of rigid boundaries on both $\phi_{ij,1}$ and $\phi_{ij,2}$ and is given by the sum of $\phi'_{ij,1}$ and $\phi'_{ij,2}$ ($\phi_{ij,w} = \phi'_{ij,1} + \phi'_{ij,2}$). The near-wall corrections $\phi'_{ij,1} + \phi'_{ij,2}$ have the form

$$\begin{aligned} \phi'_{ij,1} &= c'_1 \rho \frac{\varepsilon}{k} \left[\; \overline{u_k u_m} n_k n_m \delta_{ij} - \frac{3}{2} \overline{u_k u_i} n_k n_j - \frac{3}{2} \overline{u_k u_j} n_k n_i \; \right] \cdot f \left[\frac{\ell_t}{x_n} \right] \\ \phi'_{ij,2} &= c'_2 \left[\; \phi_{km,2} n_k n_m \delta_{ij} - \frac{3}{2} \phi_{ik,2} n_k n_j - \frac{3}{2} \phi_{jk,2} n_k n_i \; \right] \cdot f \left[\frac{\ell_t}{x_n} \right] \end{aligned}$$

where n_i is the unit vector in the "i"-direction normal to the wall (if present). The function $f[\ell_t/x_n]$ is a damping function, described in greater detail in Ref. [13], which reduces the effect of the wall correction with increasing distance from the wall, and has the form $f = k^{3/2}/(2.55 x_n \varepsilon)$ where x_n is the distance normal to the wall. Standard values on the constants have been used [10]: $(c_1, c_2, c'_1, c'_2) = (1.8, 0.6, 0.5, 0.3)$.

The turbulent diffusion of D^T_{ij} is modelled based on the Generalized Gradient Diffusion Hypothesis, (GGDH) proposed by Daly & Harlow [14] and is given as

$$D^T_{ij} = \frac{\partial}{\partial x_k} \left(c'_s \rho \overline{u_\ell u_k} \frac{k}{\varepsilon} \frac{\partial \overline{u_i u_j}}{\partial x_\ell} \right) \quad (3)$$

with $c'_s = 0.11$.

The standard ε-equation in the RSTM has the form:

$$\frac{\partial}{\partial x_j}\left(\rho U_j \varepsilon\right) = D_\varepsilon + \frac{\varepsilon}{k}\left(c_{1\varepsilon} P_k - c_{2\varepsilon}\rho\varepsilon\right) \tag{4}$$

with $(c_{1\varepsilon}, c_{2\varepsilon}) = (1.45, 1.9)$. The diffusion term D_ε is, as for the Reynolds stresses, calculated using GGDH (see Eq. 3) using $c_s' = c_\varepsilon = 0.18$.

In order to describe the turbulent heat fluxes, both the eddy-viscosity concept (used in the $k-\varepsilon$ predictions), and the GGDH model (used in the RSTM predictions) are applied. These modelling approaches may be expressed as:

$$(-\rho\overline{u_j\theta})_{EVM} = \left(\frac{\mu_t}{Pr_t}\frac{\partial T}{\partial x_j}\right) ; \qquad (-\rho\overline{u_j\theta})_{GGDH} = \rho c_\theta \frac{k}{\varepsilon}\overline{u_i u_j}\frac{\partial T}{\partial x_i} \tag{5}$$

where the values of Pr_t and c_θ are 0.9 and 0.3, respectively. Eq. 5 is used all the way to the wall.

3.1. Near-Wall Treatment

The low-Re Reynolds Stress model proposed by Shima [1] has been employed. The constants in the near-wall region have the form:

$$\begin{aligned}
c_1 &= 1 + 2.58AA^{1/4}\left\{1 - \exp\left[-\left(0.0067R_T\right)^2\right]\right\};\ c_2 = 0.75A^{\frac{1}{2}} \\
c_1' &= -\frac{2}{3}c_1 + 1.67;\ c_2' = \max\left\{2\left(c_2 - 1\right)/3 + \frac{1}{2}, 0\right\}/c_2;\ R_T = \frac{k^2}{\nu\varepsilon} \\
A &= 1 - \frac{9}{8}\left(A_2 - A_3\right);\ A_2 = a_{ik}a_{ki};\ A_3 = a_{ik}a_{kj}a_{ji};\ a_{ij} = \left(\overline{u_i u_j} - \frac{2}{3}\delta_{ij}k\right)/k
\end{aligned}$$

Since our experience of two-layer models is very good [15–18] we have chosen not to use the ε equation given in Ref. [1], but to use a two-layer approach for the dissipation term. Thus in the near-wall region the sinks in the $\overline{u_i u_j}$ equations are not determined from a transport equation, but from a prescribed length-scale distribution, i.e.

$$\varepsilon = \frac{k^{3/2}}{\ell_\varepsilon};\ \ell_\varepsilon = C_\ell n\left[1 - \exp\left(-\frac{Re_n}{A_\mu}\right)\right];\ Re_n = \frac{\rho\sqrt{k}n}{\mu} \tag{6}$$

where n is the normal distance from the wall, $A_\mu = 50.5$, and Re_n is the turbulent Reynolds number, which, in contrast to the original van Driest function, does not involve the friction velocity u^* and, hence, is valid also for separated flows. The constant C_ℓ is chosen as:

$$C_\ell = \frac{3}{4}\kappa C_\mu^{-3/4} \tag{7}$$

where C_μ is the same constant as in the standard $k-\varepsilon$ model ($= 0.09$) and κ is the von Kárman constant ($= 0.42$). The expression for ℓ_ε in Eq. 6 is the same as the formula used for ℓ_μ in Refs. [19,20] in their two-equation models. The coefficient C_ℓ in Eq. 7 has in the present work been optimized in plane channel flow (experiments by Laufer [21]), and it was found suitable to pre-multiply the coefficient C_ℓ by $\frac{3}{4}$ compared to the formulae used in Refs. [19,20].

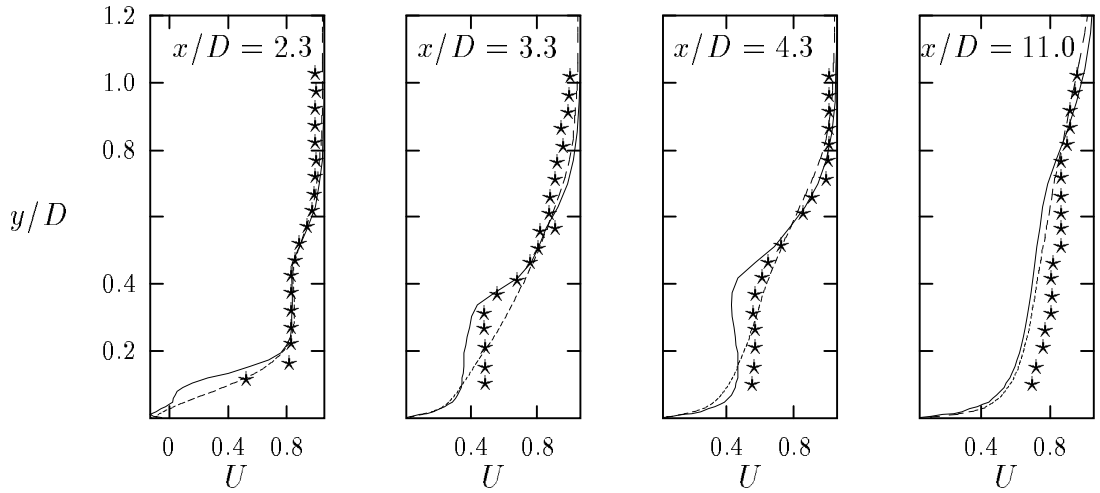

Figure 3: U velocities in the symmetry plane $z = 0$. ——, RSTM; − − −, two-layer $k - \varepsilon$ model; $\star$, experiments by Jubran [2].

To summarize, close to the wall in the viscosity affected region we use the low-Re RSTM and the dissipation ε is computed from Eq. 6, and outside this region (the fully turbulent region) the high-Re RSTM is used and the standard ε equation is solved (Eq. 4). The matching line between these two regions is taken to be along a fixed grid line in the fully turbulent region ($Re_n \simeq 200$). At the walls of the holes, standard wall functions have been used.

A detailed description of the numerical implementation into the code can be found in Refs. [15],[16].

4. Results

A grid with $158 \times 67 \times 42$ nodes is used, see Fig. 2. The point $(x, y, z) = (0, 0, 0)$ in the computational domain, refers to the leading edge of the jet exit, see Fig. 1 The hole diameter D is 19.4 mm, the free stream velocity U_o is 10 m/s and symmetry conditions are applied at $z/D = 0.0$, $z/D = 1.5$ and $y/D = 6$. Fully developed pipe flow is prescribed at the inlet of the jets which are placed 6 diameters upstream of their exit into the freestream. The inlet boundary condition for the free stream is set according to experiments and placed $8D$ upstream of the leading edge of the jet exit. The outlet boundary is applied at $x/D = 25$, where the streamwise derivatives are set to zero for all variables.

The distribution of mean velocity profiles is shown in Figs. 3 and 4, and as can be seen the velocities predicted with RSTM are in better agreement with experiments than those predicted with the $k - \varepsilon$ model. This probably reflects the sensitivity of the RSTM to streamline curvature and anisotropic turbulence (for discussion of streamline curvature, see Refs. [17,18]).

The results of film-cooling effectiveness $\Theta = (T_w - T_{free})/(T_{jet} - T_{free})$ at three spanwise positions in the flow are shown in Fig. 5. By definition of the adiabatic film-cooling

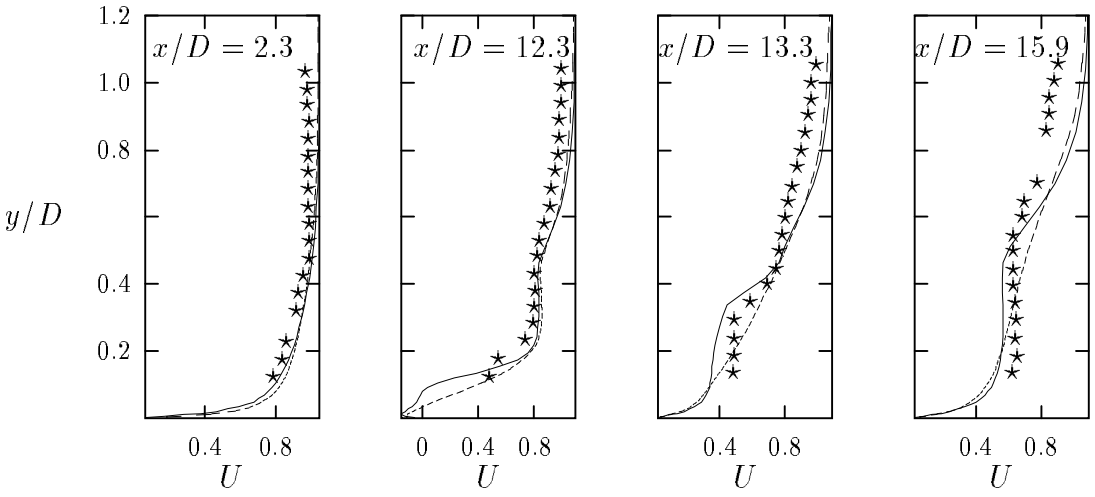

Figure 4. U velocities in plane $z/D = 1.5$. For legend, see Fig. 3

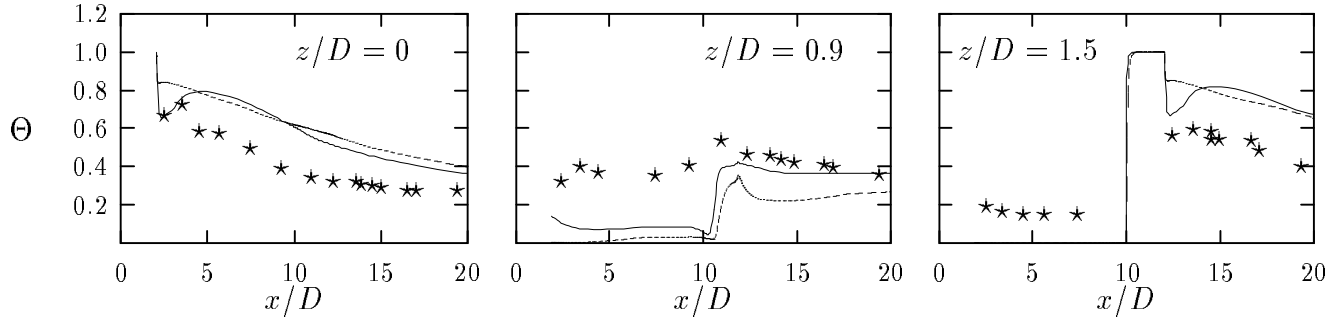

Figure 5. Film-cooling effectiveness Θ. For legend, see Fig. 3.

effectiveness, Θ, must assume the value 1 at the holes. The measured values show that a rapid mixing behind the hole at $z/D = 1.5$ is taking place since Θ is well below one immediately downstream of the hole. The measured levels of Θ at $z/D = 0.9$ and at $z/D = 1.5$ for $x/D \leq 10$ (i.e. upstream of the second jet) are remarkably high. The fact that Θ in the experiments is lower along the symmetry lines downstream of both jet exits ($z = 0$ in Fig. 5a and at $z/D = 1.5$ in Fig. 5c) indicates that the spanwise spreading is higher in the experiments than in the predictions. The RSTM predictions give a slightly higher spreading than $k - \varepsilon$, which is clearly seen in Fig. 5b ($z/D = 0.9$).

In Figs. 6 and 7 the predicted velocity vectors in two planes are shown. The recirculation bubble is, as can be seen, very small. The extent of the recirculation bubble (defined as where the skin-friction in the x direction is negative) is $0.5D$ in the streamwise direction (downstream the trailing edge of the jet exit) and $0.2D$ in the spanwise direction. Although there is no separation further away from the symmetry plane, the U velocities profiles have a inflexion point, at least up to $z/D = 0.5$. Looking at the velocity field

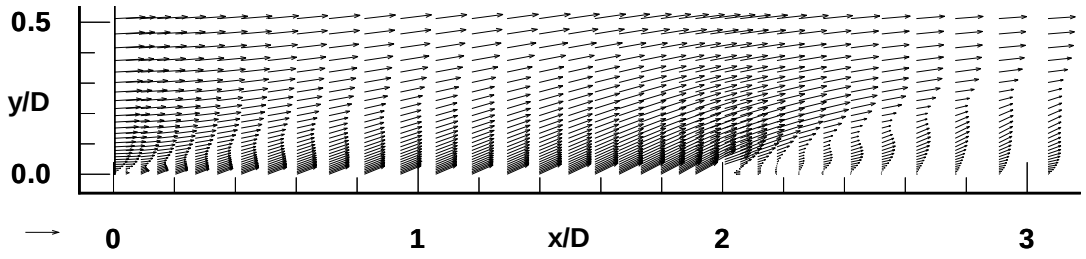

Figure 6. Velocity vectors in symmetry plane $z = 0$. RSTM. Reference vector in lower left corner $U_{ref} = 10$.

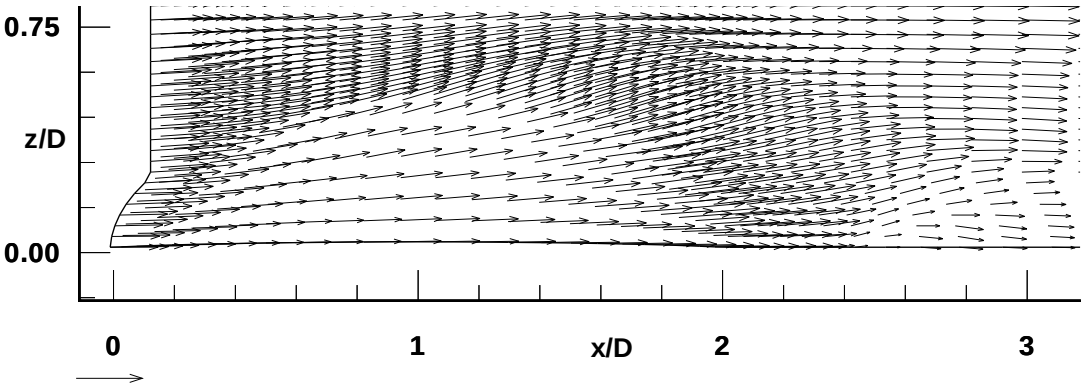

Figure 7. Velocity vectors in horizontal plane at $y/D = 0.15$. RSTM. Reference vector in lower left corner $U_{ref} = 10$

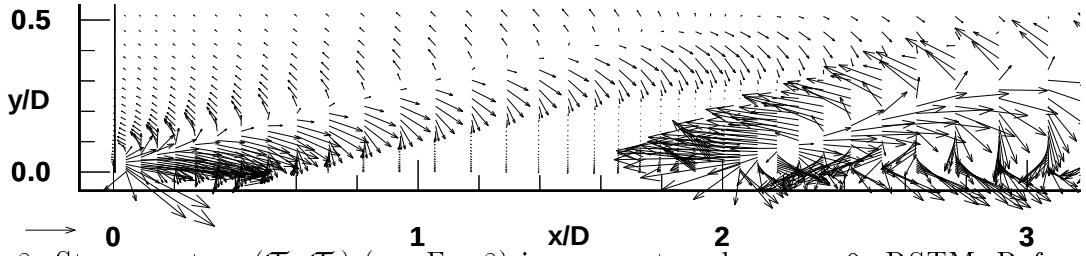

Figure 8: Stress vectors $(\mathcal{T}_x, \mathcal{T}_y)$ (see Eq. 8) in symmetry plane $z = 0$. RSTM. Reference vector in lower left corner $\mathcal{T}_{ref} = 500$

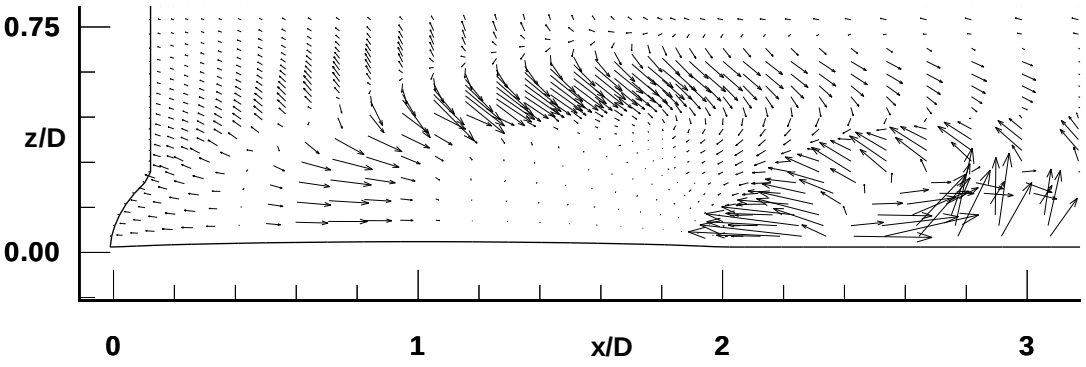

Figure 9: Stress vectors $(\mathcal{T}_x, \mathcal{T}_z)$ (see Eq. 8) in horizontal plane at $y/D = 0.15$. RSTM. Reference vector in lower left corner $\mathcal{T}_{ref} = 500$

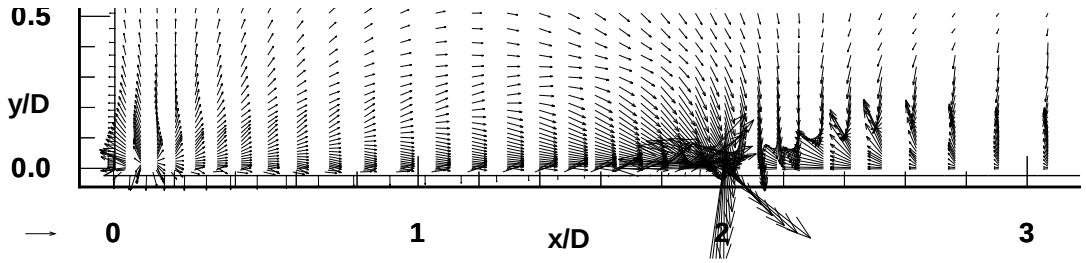

Figure 10. Pressure vectors $(-\partial p/\partial x, -\partial p/\partial y)$ in symmetry plane $z = 0$. RSTM. Reference vector in lower left corner $\mathcal{T}_{ref} = 1500$

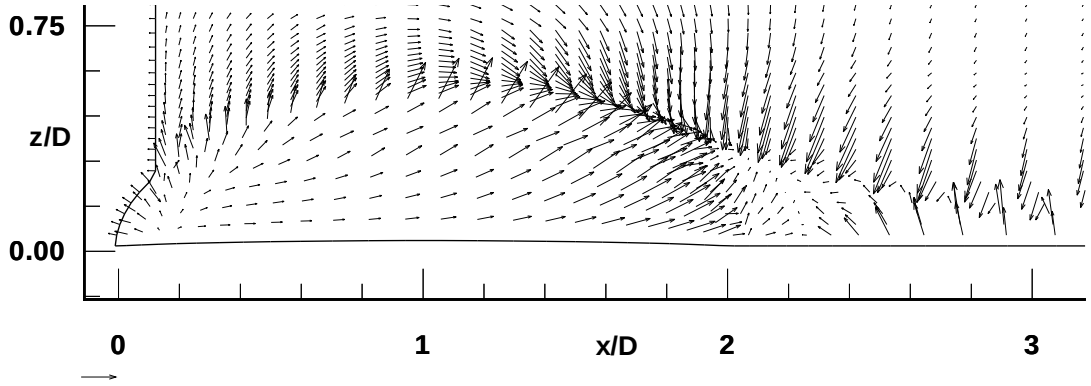

Figure 11. Pressure vectors $(-\partial p/\partial x, -\partial p/\partial z)$ in horizontal plane at $y/D = 0.15$. RSTM. Reference vector in lower left corner $\mathcal{T}_{ref} = 1500$

from above (Fig. 7) reveals that the jet does not influence the free flow very much. There is a weak W velocity component downstream of the leading edge of the jet exit. Close to the symmetry plane downstream of the jet exit at $x/D \simeq 2.6$ there is an increase in W. This seems to be related to the disappearance of the inflexion point in the U velocity profile (see Fig. 6) which creates a spanwise velocity component.

It is valuable to compare the relative influence of pressure and stresses on the flow field [17]. It is really the *gradients* of the stresses which we are interested in rather than the stresses themselves, because it is the gradients that enter the momentum equations. One of the first questions we must answer when working on turbulence modelling is: are the stresses (i.e the diffusion terms) important or is the flow field driven by pressure forces? In Figs. 8-11 the pressure gradient vectors $-\nabla p$ and stress gradient vectors $\boldsymbol{\mathcal{T}}$

$$\mathcal{T}_x = -\frac{\partial \overline{u^2}}{\partial x} - \frac{\partial \overline{uv}}{\partial y} - \frac{\partial \overline{uw}}{\partial z};\ \mathcal{T}_y = -\frac{\partial \overline{uv}}{\partial x} - \frac{\partial \overline{v^2}}{\partial y} - \frac{\partial \overline{vw}}{\partial z};\ \mathcal{T}_z = -\frac{\partial \overline{uw}}{\partial x} - \frac{\partial \overline{vw}}{\partial y} - \frac{\partial \overline{w^2}}{\partial z} \qquad (8)$$

are presented for two planes. In the symmetry plane ($z = 0$, Fig. 8) we can see that the stresses above the jet exit are generated in the shear layer (approximately $0 < x/D < 1$) which is formed when the boundary layer in the approaching free stream is disappearing when mixing with the flow from the jet. This shear layer is clearly visible in Fig. 6

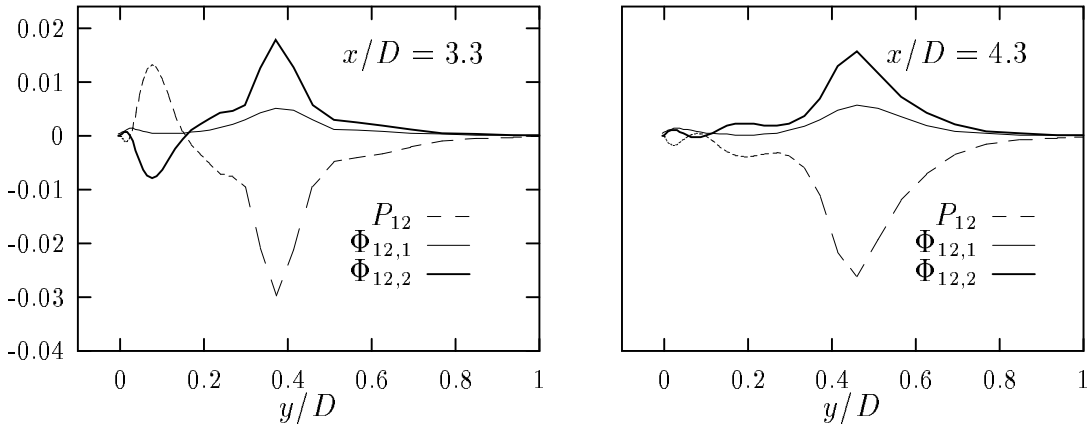

Figure 12. The largest terms in the $\overline{uv}$-equation in the symmetry plane $z = 0$ at two different x stations. RSTM.

and corresponds to the points where the U velocity profiles attain their minimum. In this shear layer the stress gradient vectors are of comparable magnitude to the pressure gradient vectors (note that the vectors in Figs. 8, 9 have been magnified by approximately a factor of two more than the vectors in Figs. 10, 11). Downstream of the trailing edge of the jet exit we have both large stress gradient vectors and pressure gradient vectors. Note that in both shear layers (the one after the leading edge and the one after the trailing edge) the component of $\boldsymbol{\mathcal{T}}$ normal to the shear layer changes sign across the shear layer. This is because the shear stress in a coordinate system aligned with the shear layer reaches its maximum in the shear layer (where the U-velocity attain its minimum, see Fig. 6) and thus its gradient changes sign. Studying the vectors fields from above, we see that also here the magnitude of the stress gradient vectors (Fig. 9) are comparable to the pressure gradient vectors (Fig. 11).

Consider a line in an approximate form of a quarter of a circle (origin at $z = 0, x/D \simeq 1.4$, Fig. 9) starting at $x/D \simeq 0.8, z = 0$ and ending after 90^o (clock-wise) at $x/D \simeq 1.6, z/D \simeq 0.5$. Along this line the stress gradient vectors are large. This line corresponds to the boundary layers formed at the walls of the hole. The velocity gradients and the stresses are convected by the jet and as a result we see large gradients of stresses.

Much work is going on in turbulence modelling on the development of modelling the pressure strain terms in Eq. 2. It is therefore interesting to study the relative influence of these terms in the stress equations. In Fig. 12 the slow term $\Phi_{12,1}$ and the rapid term $\Phi_{12,2}$ are compared to the production term P_{12}. It is seen that the rapid term is considerably larger than the slow one. This was also found in [22], when studying two-dimensional flow over a hill using Reynolds stress models.

5. Conclusion

The three-dimensional flow in a double-hole arrangement has been studied. The configuration is relevant for effusion cooling applications. A low-Re variant of an RSTM has been employed. The computed results have been compared with experiments and calculations obtained with a two-layer $k-\varepsilon$ model. It is found that the results obtained with the RSTM are in closer agreement with experiments than the $k-\varepsilon$ predictions.

The gradients of the stresses and the pressure gradients are studied in form of vector plots in order to evaluate their relative influence on the balance of the momentum equations. They are found to be comparable, which means that it is worth while to further develop turbulence models for this type of applications. Furthermore, the influence of the pressure strain terms in the stress equations is studied, and it is found that the rapid term is much larger than the slow one.

REFERENCES

1. N. Shima, Proc. 7th Symp. Turb. Shear Flows, Stanford, pp. 5.3.1−5.3.6 (1989).
2. B.A. Jubran, J. Turbomach., 111 (1989), 502.
3. N.Z. Inze and M.A. Leschziner, Proc. Engineering Turbulence Modelling and Experiments, Eds. W. Rodi and E.N. Ganić, Elsevier, pp. 155-164 (1990).
4. N.Z. Inze and M.A. Leschziner, AGARD Symp. on Computation and Experimental Assessment of Jets in Cross-Flow, Paper 23, Winchester, 1993.
5. L. Davidson L. and B. Farhanieh, Chalmers Univ.of Technology, Rept. 92/4 (1992).
6. J.P. Van Doormal and G.D. Raithby, Numerical Heat Transfer, 7 (1984), 147.
7. C.M. Rhie and W.L. Chow, AIAA J, 21 (1983) 1525.
8. B.P. Leonard, Comp. Meth. Appl. Mech. Engng, 19 (1979) 59.
9. B. van Leer, J. Comp. Phys., 14 (1974) 361.
10. M.M. Gibson and B.E. Launder, J. Fluid Mech., 86 (1978) 491.
11. J.C. Rotta, Zeitschrift für Physik, 129 (1951), 547.
12. D. Naot, A. Shavit and M. Wolfshtein, Israel J. Techn., 8 (1970) 259.
13. P.G. Huang and M.A. Leschziner, Proc. 5th Symp. Turb. Shear Flows, Cornell University, pp. 20.7−20.12 (1985).
14. B.J. Daly and F.H. Harlow, Physics of Fluids, 13 (1970) 2634.
15. L.S. Jansson and L. Davidson, Proc 2nd European Comp. Fluid Dynamics '94, pp. 535-542, Eds. S. Wagner *et al.*, Stuttgart, John Wiley & Sons (1994).
16. L.S. Jansson, Phd thesis, Thermo and Fluid Dynamics, Chalmers University of Technology, Gothenburg (1994).
17. L. Davidson, ASME J. Fluid Engng., 117 (1995) 50.
18. L. Davidson, Computers & Fluids, 24 (1995) 253.
19. L.H. Norris and W.C. Reynolds, Rept. No. FM-10, Dept. Mech. Eng., Stanford (1975).
20. H.C. Chen and V.C. Patel, AIAA J., 26 (1988) 641.
21. J. Laufer, NACA Rept. 1053 (1951).
22. S. Perzon, L. Davidson and M. Ramnefors, A Study of the Flow Over a Two-Dimensional Hill, unpublished results (1995).